Research Article

Muthu Rajarathinam, Muhammad Ijaz Khan*, Barno Sayfutdinovna Abdullaeva, Tehseen Abbas, Fuad A. Awwad, and Emad A. A. Ismail

# Optimizing heat transport in a permeable cavity with an isothermal solid block: Influence of nanoparticles volume fraction and wall velocity ratio

https://doi.org/10.1515/phys-2024-0003
received August 22, 2023; accepted March 07, 2024

**Abstract:** This study examines the influence of wall velocity ratio on mixed convective heat transport in a permeable cavity containing an isothermal solid block at its center. The analysis considers the characteristics of various flow variables, *i.e.*, Darcy number, wall velocity ratio, Richardson number, and volume fraction of suspended nanoparticles, on heat transport and material flow characteristics. The principal equations are solved implementing the semi-implicit method for pressure linked equations algorithm, and the outcomes are compared with existing literature. The study shows that rising estimations of Darcy number, velocity ratio, Richardson number, and nanoparticles volume fraction lead to improved heat transfer rates. For example, at high Richardson number (100) and solid volume fraction (0.05), increasing the velocity ratio from 0.5 to 1.5 results in a 6% (5%) upsurge in heat transport rate. Conversely, at smaller Richardson number (0.01), the heat transport rate upsurges by 29% (28%). Similarly, at high Darcy numbers and low wall velocity ratios, a 3% (4%) escalate in heat transport rate is observed with an increase in nanoparticles concentration from 0 to 0.05, while a 9% (8%) increase in thermal performance is achieved at low Darcy numbers. The study emphasizes the importance of optimizing the combination of nanoparticles volume fraction, Darcy number, velocity ratio, and Richardson number to maximize thermal performance in the porous cavity.

**Keywords:** porous cavity, nanofluid mixed convection, isothermal block, wall velocity ratio

*** Corresponding author: Muhammad Ijaz Khan**, Department of Mathematics and Statistics, Riphah International University I-14, Islamabad, 44000, Pakistan; Department of Mechanical Engineering, Lebanese American University, Kraytem, 1102-2801, Beirut, Lebanon, e-mail: 2106391391@pku.edu.cn
**Muthu Rajarathinam:** Department of Science and Humanities, Karpagam College of Engineering, Coimbatore, 641 032, India
**Barno Sayfutdinovna Abdullaeva:** Department of Mathematics and Information Technologies, Faculty of Mathematics and Physics, Vice-Rector for Scientific Affairs, Tashkent State Pedagogical University, Tashkent, Uzbekistan
**Tehseen Abbas:** Department of Mathematics, Division of Science and Technology, University of Education, Lahore, 54770, Pakistan
**Fuad A. Awwad, Emad A. A. Ismail:** Department of Quantitative Analysis, College of Business Administration, King Saud University, P.O. Box 71115, Riyadh, 11587, Saudi Arabia

## Nomenclature

| | |
|---|---|
| $c_p$ | specific heat capacity (J kg$^{-1}$ K$^{-1}$) |
| Da | Darcy number |
| Fc | Forchheimer term |
| $G$ | acceleration due to gravity (m s$^{-2}$) |
| Gr | Grashof number |
| $K$ | permeability of the medium (m$^2$) |
| $k_{nf}$ | thermal conductivity (W m$^{-1}$ K$^1$) |
| $L$ | length of the cavity (m) |
| Nu | local Nusselt number |
| $p$ | pressure (Pa) |
| $P$ | dimensionless pressure |
| Pr | Prandtl number |
| Ra | Rayleigh number |
| Re | Reynolds number |
| Ri | Richardson number |
| $\overline{\mathrm{Nu}}$ | average Nusselt number |
| $U$, $V$ | dimensionless velocities |
| $u$, $v$ | dimensional velocities |
| $X$, $Y$ | dimensionless coordinates |
| $x$, $y$ | dimensional coordinate (m) |

## Greek symbols

| | |
|---|---|
| $\lambda$ | wall velocity ratio |

| | |
|---|---|
| $\alpha$ | thermal diffusivity ($m^2\ s^{-1}$) |
| $\tau$ | dimensionless time |
| $\nu$ | kinematic viscosity ($m^2\ s^{-1}$) |
| $\rho$ | density ($kg\ m^{-3}$) |
| $\mu$ | dynamic viscosity ($kg\ m^{-1}\ s^{-1}$) |
| $\varphi$ | wall velocity ratio |
| $\beta$ | coefficient of thermal expansion ($K^{-1}$) |
| $\theta$ | dimensionless temperature |
| $\varepsilon$ | porosity of the medium |

## Subscripts

| | |
|---|---|
| f | base fluid |
| h | hot |
| nf | nanofluid |
| p | nanoparticles |

# 1 Introduction

The presence of an isothermal block within a resonator has attracted attention due to its common occurrence in electronic packages and its various technological applications. As a result, several scientists and examiners have focused on analyzing heat/mass transport in these configurations [1]. Several studies have analyzed the heat transfer performance when an isothermal solid block is present in cavities. For example, Sun *et al.* [2] investigated natural convective heat transport in closed cavities subject to isothermal solid block at the center. Kalidasan *et al.* [3] scrutinized the heat transport characteristics of an isothermal solid block in an open-ended cavity using hybrid nanofluids. Mehmood *et al.* [4] worked on alumina-water based nanoliquids flow with forced convection phenomena and hot iso-thermal block inside a lid-driven cavity considering the characteristics of a applied magnetic field. Their findings showed that the existence of the nano-liquid and mixed convection augmented the heat transport rate. Haq *et al.* [5] scrutinized the heat transport influence of an isothermal block in a moderately heated rhombus cavity. The research demonstrates that the heat transport and fluid flow behavior were greatly influenced by isothermally heat square block.

In the last couple of decades, there has been a growing curiosity in studying heat transfer in environments where mixed convection occurs and porous walls are present. This research has applied utilizations and application in numerous thermal devices like solar panels, electronic cooling systems, building heating and cooling systems, and the food industry. Kumar *et al.* [6] focused on a research that represents the characteristics of heat transport in a porous cavity using a multigrid approach. Their findings recommend that the consolidation of shear force and buoyancy effects in mixed convection leads to improved heat propagation. Sivasankaran and Pan [7] scrutinized the characteristics of non-uniform thermal boundary conditions (BC) on mixed convection flow and heat transport in a lid-driven permeable cavity. They observed that non-uniform heating of double side walls resulted in advanced heat transport rates compared to non-uniform heating of a single wall. Moria [8] established a mathematical model to explore natural convective flow using porous medium and solid blocks. Their consequences exhibited an important augmentation in heat transport performance when porous materials were present, especially at high Rayleigh numbers. Colak *et al.* [9] further investigated a similar problem by incorporating a heated porous block into the mixed convection state. They found that the permeable variable played an important role in improving heat transport by governing vortex formation.

The utilization of nanofluids in electronic devices presents a novel method to enhance heat transfer efficiency [10–12]. Various studies have explored the consequences of nanomaterials for cooling performance in lid-driven permeable cavities. Recently, Begum *et al.* [13] and Hussain *et al.* [14] conducted numerical simulations and demonstrated that nanofluids can greatly improve cooling rates due to their superior thermal conductivity. Nithyadevi *et al.* [15] investigated different factors influencing enhanced heat transfer, such as nanofluid char mixed convection, nanofluid properties, and wall speed ratio, highlighting the importance of the wall speed ratio in achieving significant heat transfer enhancement. In a latest research, Alomari *et al.* [16] inspected heat transport phenomenon in a lid-driven cavity nanofluid flow in the presence of porous layer. Their obtained consequences designated that heat transport rates increase with higher mixed convection and forced convection parameters, nanoparticle concentrations, and porous parameters, with a notable 64% enhancement in heat transport rate at rising Reynolds numbers. Long *et al.* [17] examined macroscopic and mesoscopic characteristics of sintered silver nanomaterials *via* crystal plasticity FEM.

Investigating the combined effects of mixed convection, wall velocity ratio and nanomaterials presents motivating exploration query that has not been extensively explored. Heat transport phenomenon in the presence of isothermal solid block is particularly relevant in various industrial utilizations involving porous media. The aim of this exploration work was to address this research gap by examining the impact of an isothermal solid block on thermal behavior and fluid flow, as well as the potential heat transport rate enhancement with the use of Cu-water nanofluids. Additionally, the study will explore the influence of wall velocity ratio on heat transport rate in the

presence of the isothermal block and quantify the heat transfer rate increase with the addition of copper nanoparticles. Numerical analysis will be employed to examine the behavior of convective heat transport in a permeable cavity with an isothermal solid block, considering the wall velocity ratio. The findings of this study are expected to provide valuable insights for the design of electronic equipment and contribute to reducing energy ingesting in industrial sceneries.

## 2 Modeling of the problem

In our ongoing research, we have chosen a porous cavity with a size of $L$ as the basis for our study. Inside the cavity, we have introduced a nanofluid consisting of Cu and water (Figure 1). In the graphical abstract, $T_h$ and $T_c$, respectively characterize the temperature of left and right vertical walls of the cavity, where $T_h > T_c$. Furthermore, the top and bottom walls of the cavity are considered adiabatic. At the center of the cavity, there is a heated square block with an isothermal temperature $\left(\frac{T_h + T_c}{2}\right)$. The size of the block is given by $\frac{L}{4}$. Let us assume that the top wall is moved with constant velocity $U_t = U_0$ from left to right. But the bottom wall, can slide with a velocity $U_b$, either in the same direction or opposite direction, where $U_b = \lambda U_0$, and ($\lambda = U_b/U_0$) stands for variable wall velocity ratio. In this study, we make the following assumptions to model the flow equations:

- Neglecting induced electric current, viscous dissipation, and Joule heating effects.
- Assuming negligible radiative heat transport between the cavity walls.
- Considering the permeable medium to be homogeneous, isotropic, and in thermal equilibrium with the nano-fluid.

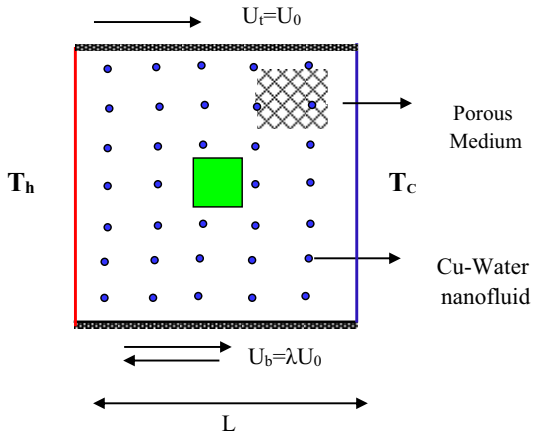


**Figure 1:** Graphical display of current research.

- Assuming the nano-fluid flow to be unsteady, laminar, incompressible, and Newtonian.
- Treating the nanoliquid as a single-phase system with thermal equilibrium between the nanoparticles and fluid.
- Given constant physical characteristics of the nanofluid, except for density changes in the buoyancy term using the Boussinesq approximation.

In the presence of above assumptions, the principal flow expressions are listed as follows [6,15,18]:

$$\frac{\partial U}{\partial X} + \frac{\partial V}{\partial Y} = 0, \tag{1}$$

$$\begin{aligned}&\frac{1}{\varepsilon}\frac{\partial U}{\partial \tau} + \frac{1}{\varepsilon^2}\left(U\frac{\partial U}{\partial X} + V\frac{\partial U}{\partial Y}\right)\\ &= -\frac{\partial P}{\partial X} + \frac{1}{\varepsilon}\frac{\nu_{nf}}{\nu_f}\frac{1}{\mathrm{Re}}\nabla^2 U - \frac{\mathrm{Fc}}{\sqrt{\mathrm{Da}}}U\sqrt{U^2+V^2}\\ &\quad - \frac{\nu_{nf}}{\nu_f}\frac{1}{\mathrm{Re}}\frac{U}{\mathrm{Da}},\end{aligned} \tag{2}$$

$$\begin{aligned}&\frac{1}{\varepsilon}\frac{\partial V}{\partial \tau} + \frac{1}{\varepsilon^2}\left(U\frac{\partial V}{\partial X} + V\frac{\partial V}{\partial Y}\right)\\ &= -\frac{\partial P}{\partial Y} + \frac{1}{\varepsilon}\frac{\nu_{nf}}{\nu_f}\frac{1}{\mathrm{Re}}\nabla^2 V - \frac{\nu_{nf}}{\nu_f}\frac{1}{\mathrm{Re}}\frac{V}{\mathrm{Da}} + \frac{\beta_{nf}}{\beta_f}Ri\,\theta\\ &\quad - \frac{\mathrm{Fc}}{\sqrt{\mathrm{Da}}}V\sqrt{U^2+V^2},\end{aligned} \tag{3}$$

$$\frac{\partial \theta}{\partial \tau} + U\frac{\partial \theta}{\partial X} + V\frac{\partial \theta}{\partial Y} = \frac{\alpha_{nf}}{\alpha_f}\frac{1}{\mathrm{Re}\,\mathrm{Pr}}\nabla^2\theta, \tag{4}$$

where $\mathrm{Fc}\left(=\frac{1.75}{\sqrt{150}\,\varepsilon^{3/2}}\right)$ The list of dimensionless parameters that appeared in the above equations are $\mathrm{Ri}(=\mathrm{Gr}/\mathrm{Re}^2)$ characterizes the Richardson number, $\mathrm{Gr}\left(=\frac{g\beta_f \Delta T L^3}{\nu_f^2}\right)$ is the Grashof number, $\mathrm{Da}\left(=\frac{K}{L^2}\right)$ is the Darcy number, $\mathrm{Re}\left(=\frac{U_0 L}{\nu_f}\right)$ describes the Reynolds number, and $\mathrm{Pr}\left(=\left(\frac{\nu}{\alpha}\right)_f\right)$ is the Prandtl number.

The proposed boundary constraints are [4,19]:

$$\left.\begin{aligned}&\tau = 0: \quad U = V = 0, \quad \theta = 0, \quad X, Y \in [0,1]\\ &\tau > 0: \quad U = V = 0, \quad \theta = 1, \quad X = 0, \quad Y \in [0,1],\\ &\qquad U = 0, V = 0, \quad \theta = 0, \quad X = 1, \quad Y \in [0,1],\\ &\qquad U = 1, V = 0, \quad \frac{\partial \theta}{\partial Y} = 0, \quad X \in [0,1], \quad Y = 1,\\ &\qquad U = \lambda, V = 0, \quad \frac{\partial \theta}{\partial Y} = 0, \quad X \in [0,1], \quad Y = 0.\end{aligned}\right\} \tag{5}$$

At the block surface,

$$\left.U = 0, V = 0, \theta = 0.5.\right\} \tag{6}$$

**Table 1:** Thermo-physical characteristics of base fluid and nanoparticles [18]

| Physical attributes | Water | Cu |
|---|---|---|
| $\beta$ (1/K) | $21 \times 10^{-5}$ | $1.67 \times 10^{-5}$ |
| $k$ (W/m K) | 0.613 | 401 |
| $\rho$ (kg/m$^3$) | 997.1 | 8,933 |
| $c_p$ (J/kg K) | 4,179 | 385 |

The mathematical form of the transport units of the nanofluids are [4,17]

$$\left.\begin{aligned} &\frac{\rho_{nf}}{\rho_f} = (1-\phi) + \phi\left(\frac{\rho_p}{\rho_f}\right), \alpha_{nf} = \left(\frac{k}{\rho c_p}\right)_{nf}, \\ &\frac{k_{nf}}{k_f} = \frac{k_p(1+2\phi) + 2k_f(1-\phi)}{k_p(1-\phi) + k_f(2+\phi)} \\ &\frac{(\rho c_p)_{nf}}{(\rho c_p)_f} = (1-\phi) + \phi\frac{(\rho c_p)_p}{(\rho c_p)_f}, \\ &\frac{(\rho\beta)_{nf}}{(\rho\beta)_f} = (1-\phi) + \phi\frac{(\rho\beta)_p}{(\rho\beta)_f} \end{aligned}\right\}. \tag{7}$$

In the above equation, $\rho c_p$, $\rho_{nf}$, $\beta_{nf}$, $k_{nf}$, and $\alpha_{nf}$ denote heat capacity, nanofluid density, thermal expansion, thermal conductivity, and thermal diffusivity. Also, $f$ stands for fluid in the subscripts, $p$ denotes the nanoparticles in the subscripts, and $\phi$ denotes the nanoparticles volume fraction (Table 1).

### 2.1 Nusselt number

Mathematically, the Nusselt number for the present flow problem is defined as [4,17]

$$\mathrm{Nu} = -\left(\frac{k_{nf}}{k_f}\right)\frac{\partial\theta}{\partial X}. \tag{8}$$

The mathematical expression for the average Nu in the flow of liquid layer adjacent to the hot surface of wall is addressed as [4,17].

$$\overline{\mathrm{Nu}} = \int_0^1 \mathrm{Nu}\,dY\,|_{X=0}. \tag{9}$$

## 3 Scheme procedure, grid independent test and code validation

The finite volume method is utilized to discretize the transport partial differential equations and their boundary condition. However, resolving the momentum equations (ME) is difficult due to their non-linearity and the attendance of an unknown pressure field. The pressure gradient term is included in the ME, but there is no separate equation to regulate the pressure. To tackle these challenges, the semi-implicit method for pressure linked equations algorithm, established by Patankar [20], is employed. The transient terms are handled with a fully implicit scheme, while the convection and diffusion terms are approximated using specific systems. The resultant system of algebraic equations is resolved using the Thomas algorithm with an iterative approach. This process is repeated until a converged solution is attained, with a chosen convergence criterion for the problem (Figures 2–4).

$$\frac{\Sigma|\phi_{i,j}^{n+1} - \phi_{i,j}^{n}|}{\Sigma|\phi_{i,j}^{n+1}|} < 10^{-5}, \tag{10}$$

In Eq. (10), $\phi$ characterizes $\theta$, $U$, or $V$.

To select a better grid size for the present study, grid independent test was performed for different mesh sizes on the average Nusselt number for the hot wall at $\phi = 0.025$, $\mathrm{Da} = 10^{-3}$ and $\mathrm{Ri} = 1.0$ which is shown in Table 2. From the table, we observed that extending the grid size from $150 \times 150$ to $200 \times 200$ results in the lowest error rate for both $\lambda = -1$ and $\lambda = 1$. Therefore, to save time, the grid size $150 \times 150$ is fixed for all simulations in this article. To verify the accuracy of the present in house computational code, the present results are compared with the previous works of Mehmood et al. [4], Jmai et al. [19] and Kumar et al. [6] as shown in Figures 2–4 respectively. These figures qualitatively reflect the comparison results, however a quantitative comparison also being carried out and are presented in Table 3 and Table 4. In these validation, the influence of solid block, wall speed ratio, the porous effect, the mixed convection effect and the presence of nanofluid in porous medium were confronted with the previous ones, and these comparison provides the enough reliability and consistency of the present in house code used here.

## 4 Discussion and analysis

In this part of the research study, we have scrutinized the influence of different pertinent flow variables on the isothermal contours, average Nusselt number, and streamlines. The parameters considered are Darcy number, wall velocity ratio, Richardson number and nanoparticles volume fraction. These parameters are varied within a specified range, while other variables, *i.e.*, porosity, Prandtl number and Reynolds number are held constant (0.6, 6.2, 100).

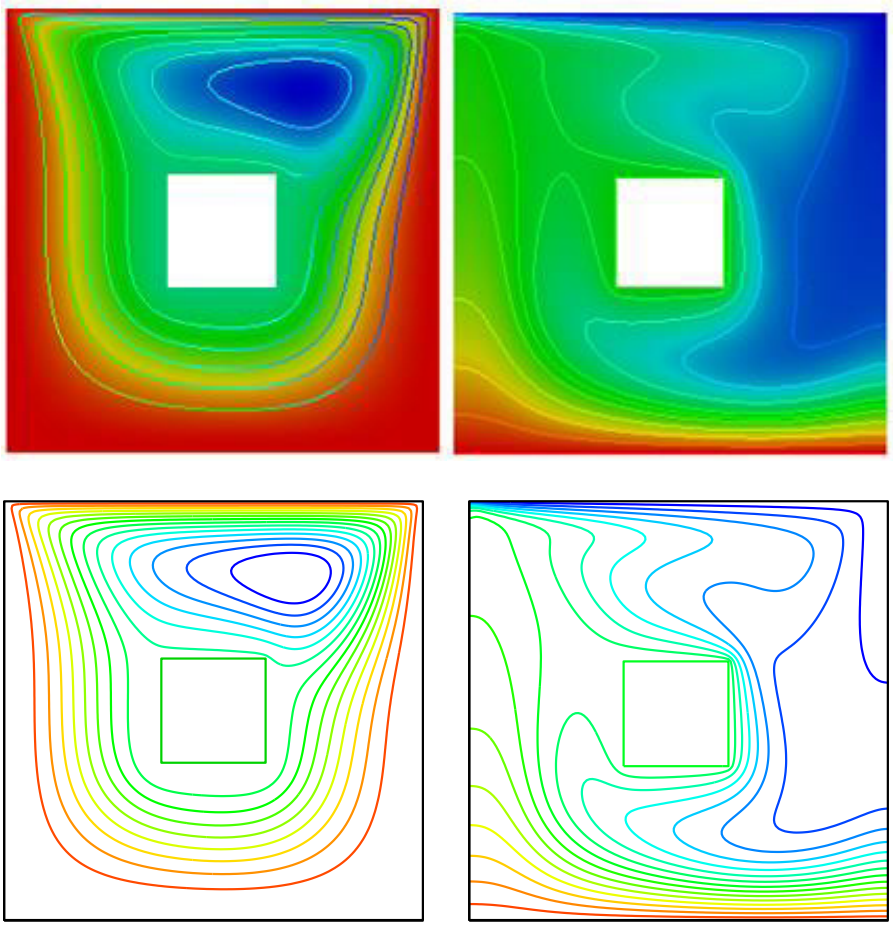

**Figure 2:** The present outcomes are compared with that in the study by Mehmood *et al.* [4] between their present findings (bottom) and their previous work at $\phi$ = 0.2, Re = 100, and Ri = 0.1.

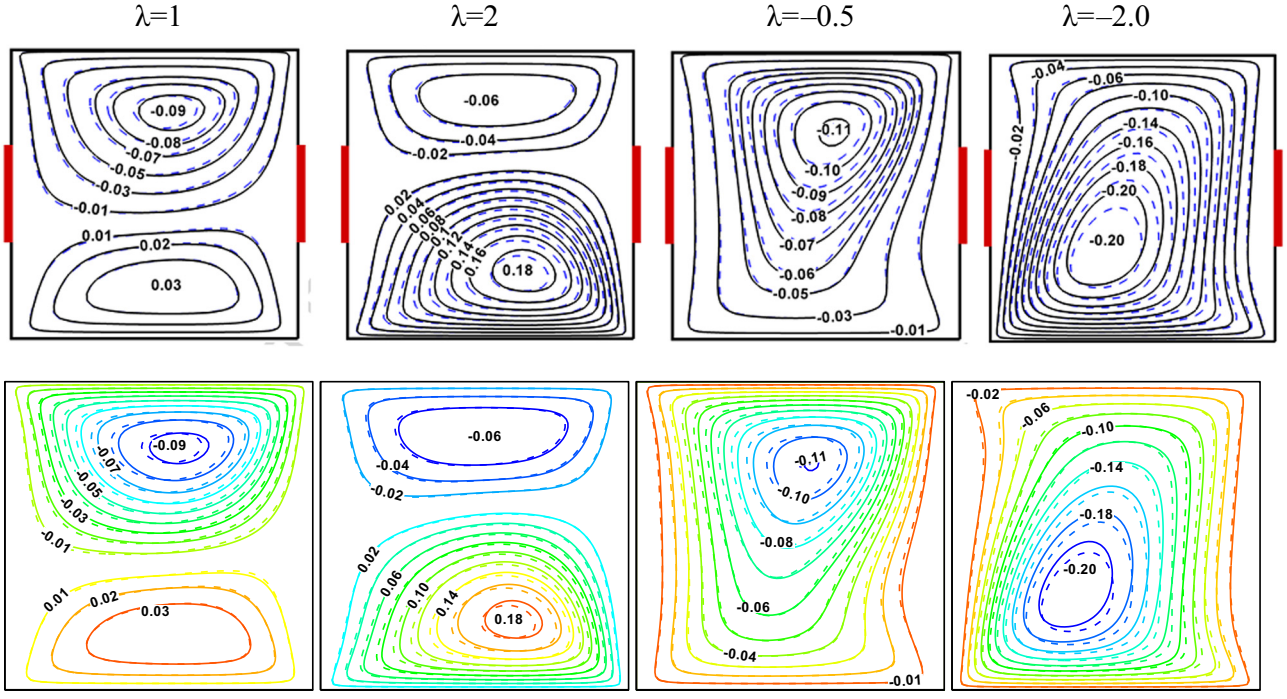


**Figure 3:** Comparative analysis of present (bottom) with Jmai *et al.* [19] (top) when Ri = 1.0.

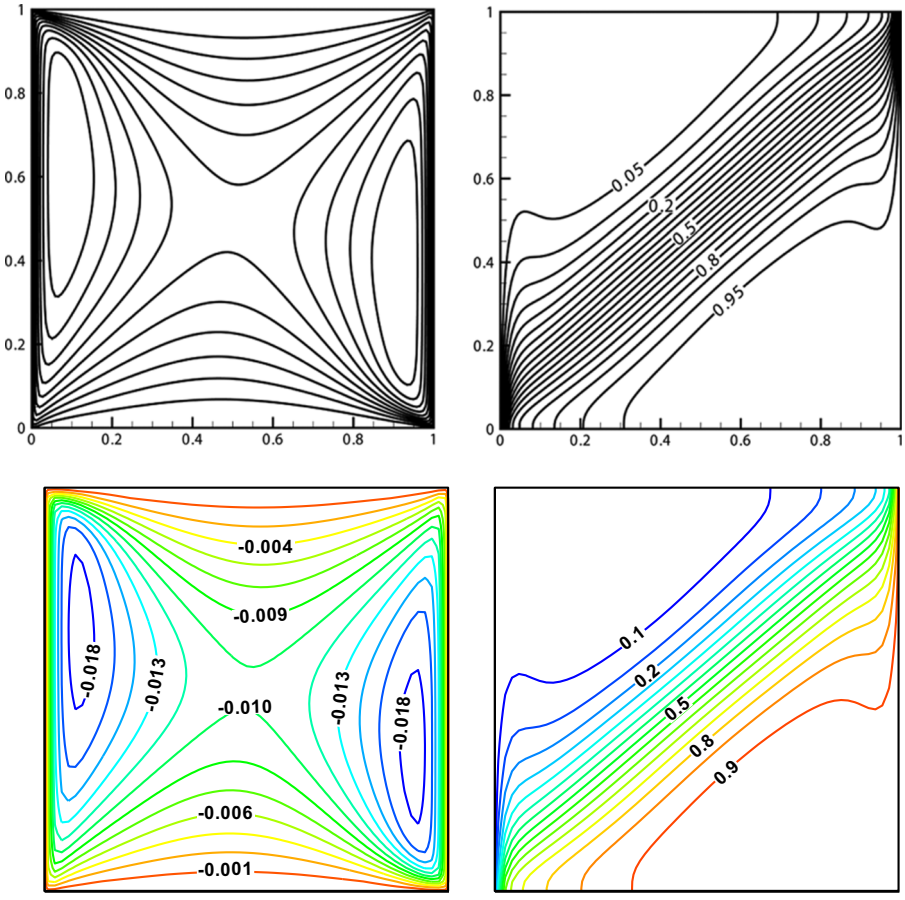


**Figure 4:** For Pr = 0.71, Ri = $10^{-2}$, $\varepsilon$ = 0.9, Da = $10^{-3}$, and $N$ = 0, the present outcomes (bottom) is compared with that in the study by Kumar *et al.* [6].

The physical illustration for the behavior of Richardson number and wall velocity ratio on the streamlines is depicted in Figure 5, while the remaining variables are considered constant. The increasing values of wall velocity ratio specifies that both bottom and top walls in the same direct direction, demonstrating conflicting shear and buoyancy forces. When Ri = 0.01, then flow is caused by only forced convection phenomenon, as a result two circular cell formation is obtained. The clockwise cell occupies a larger portion of the cavity than the anticlockwise cell. As the Richardson number rises from 0.01 to 100, the buoyancy force gains more influence compared to the shear force, resulting in a gradual reduction in the size of the counterclockwise cell. Conversely, the clockwise cell expands towards the lower wall as the buoyancy force intensifies. Additionally, increasing the wall velocity ratio enhances the counterclockwise flow in the secondary cell and leads to its gradual enlargement due to increased shear force on the bottom wall.

**Table 2:** Analysis of $\overline{\mathrm{Nu}}$ subject to grid independent approach at $\phi$ = 0.025, Da = $10^{-3}$, and Ri = 1.0

| Grid size | $\overline{\mathrm{Nu}}$ | | | |
|---|---|---|---|---|
| | $\lambda$ = 1 | Error % | $\lambda$ = −1 | Error % |
| 50 × 50 | 5.912961 | 3.01 | 7.227505 | 1.6 |
| 100 × 100 | 6.096704 | 0.98 | 7.345699 | 0.4 |
| **150 × 150** | **6.157492** | **0.2** | **7.381020** | **0.3** |
| 200 × 200 | 6.170955 | | 7.404594 | |

The bold value indicates that grid size 150 gives the lowest error % and is fixed for the computation of the present analysis.

**Table 3:** Comparative study of $\overline{\mathrm{Nu}}$ with Mehmood *et al.* [4] when $\phi$ = 0.2 and Re = 100

| Richardson number | $\overline{\mathrm{Nu}}$ | | |
|---|---|---|---|
| | Present outcomes | Mehmood *et al.* [4] | Error % |
| 0.1 | 7.6998 | 7.6910 | 0.1 |
| 1.0 | 8.6051 | 8.5651 | 0.5 |
| 10 | 11.3936 | 11.3558 | 0.3 |

**Table 4:** Comparative scrutiny of $\overline{Nu}$ subject to $\phi$ at $\varepsilon = 0.4$

| Ra | Da | $\phi$ | $\lvert\psi\rvert$ max | | | $\overline{Nu}$ | | |
|---|---|---|---|---|---|---|---|---|
| | | | [17] | Present outcomes | Error % | [17] | Present outcomes | Error % |
| $10^3$ | $10^{-2}$ | 0.0 | 0.283 | 0.282 | 0.35 | 1.007 | 1.010 | 0.29 |
| | | 0.025 | 0.264 | 0.263 | 0.37 | 1.081 | 1.090 | 0.82 |
| | | 0.05 | 0.246 | 0.245 | 0.40 | 1.160 | 1.171 | 0.93 |

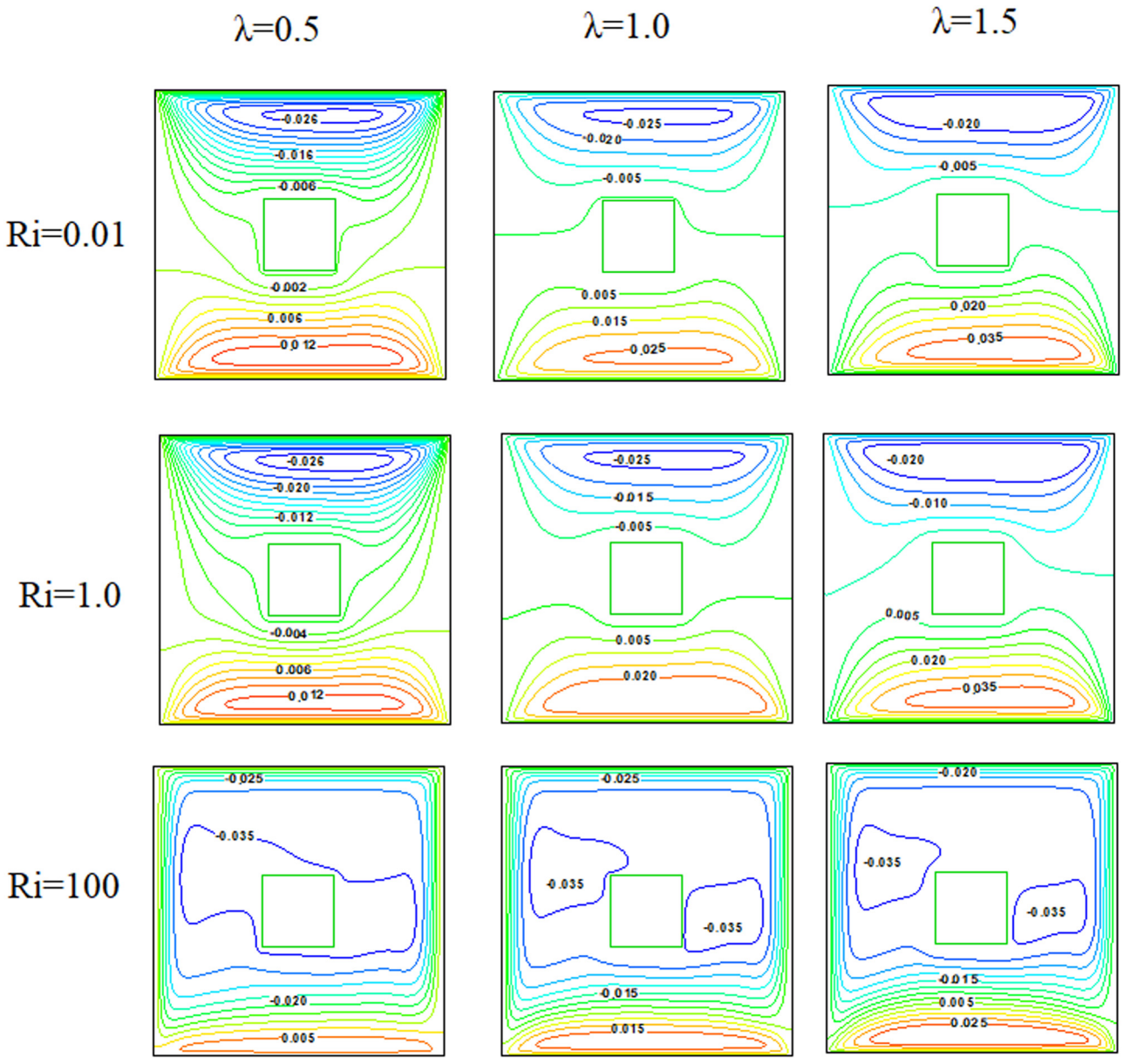


**Figure 5:** Physical interpretation of steady state streamlines *vs* Richardson number and wall speed ratio with fixed $\phi = 0.025$ and $Da = 10^{-3}$.

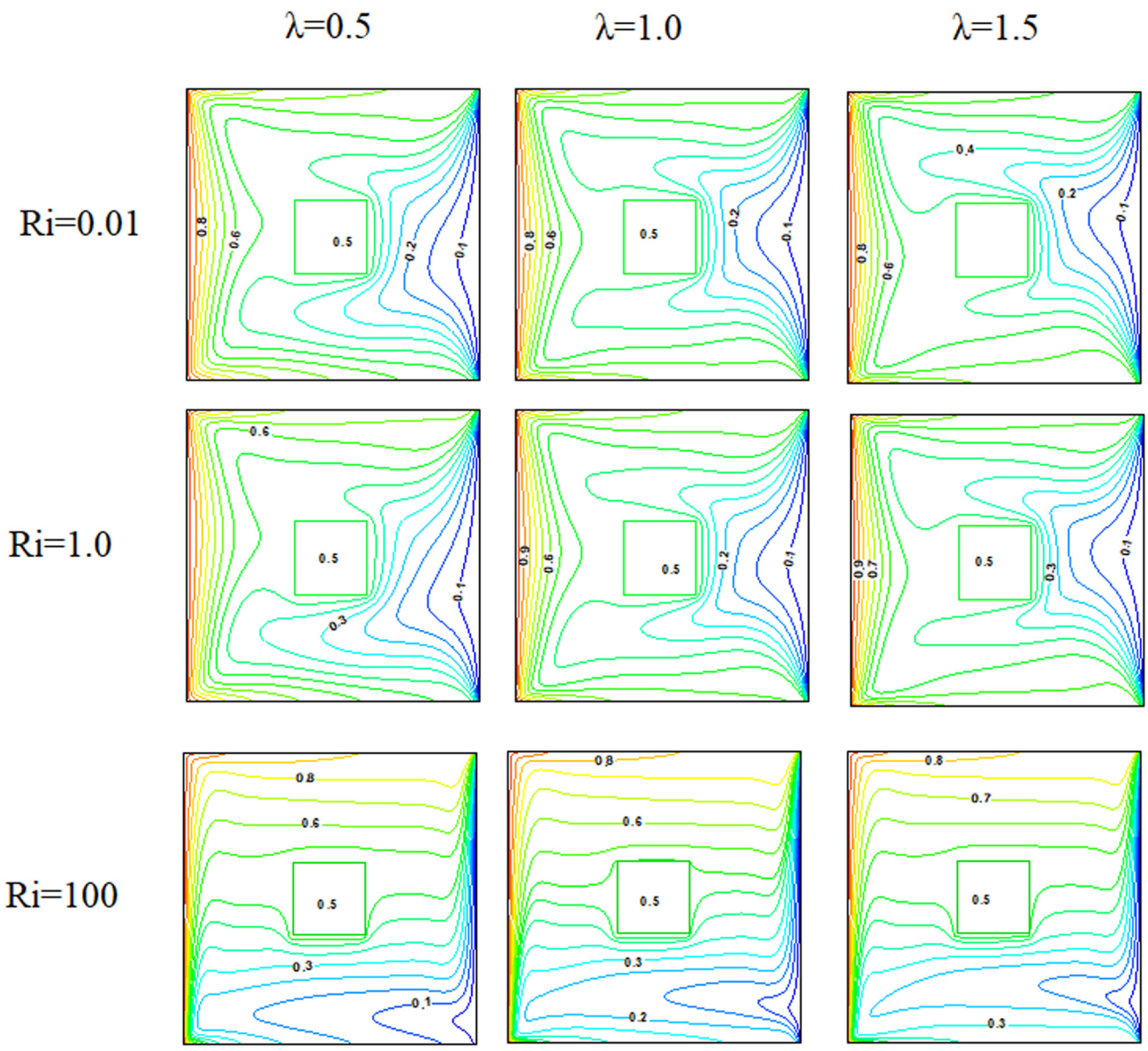


**Figure 6:** Physical interpretation of steady state isotherms *vs* Richardson number and wall speed ratio with fixed $\phi$ = 0.025 and Da = $10^{-3}$.

Figure 6 displays isotherms for various Richardson numbers and wall velocity ratios. Increasing the wall velocity ratio shifts the isotherms near the cold wall towards the left wall through the block's top surface, causing distortion near the bottom wall due to heightened shear force. A notable temperature gradient is seen near the hot vertical wall. With a higher Richardson number, isotherms tend to cluster near the active wall, indicating a dominant natural convection state. Figure 7 shows the impact of the Darcy number on streamlines, while Figure 8 depicts the effect on isotherms with a fixed Richardson number and nanoparticles volume fraction. The cavity is filled with double circulating cells near the top and bottom walls when Da = $10^{-5}$, with the rest remaining stagnant, regardless of the wall velocity ratio.

Increasing the Darcy number in a porous medium enhances its permeability, affecting the size and movement of cells within the medium. Higher Darcy numbers result in larger clockwise cells near the bottom wall and a decrease in counterclockwise cells at higher flow rates. This effect is more pronounced at lower wall speed ratios. For moderate and high wall velocity ratios, increasing the Darcy number intensifies fluid flow, creating eddies near the top and bottom right corners of the cavity. A higher wall velocity ratio leads to a stronger shear force near the moving bottom wall, increasing the size and circulation

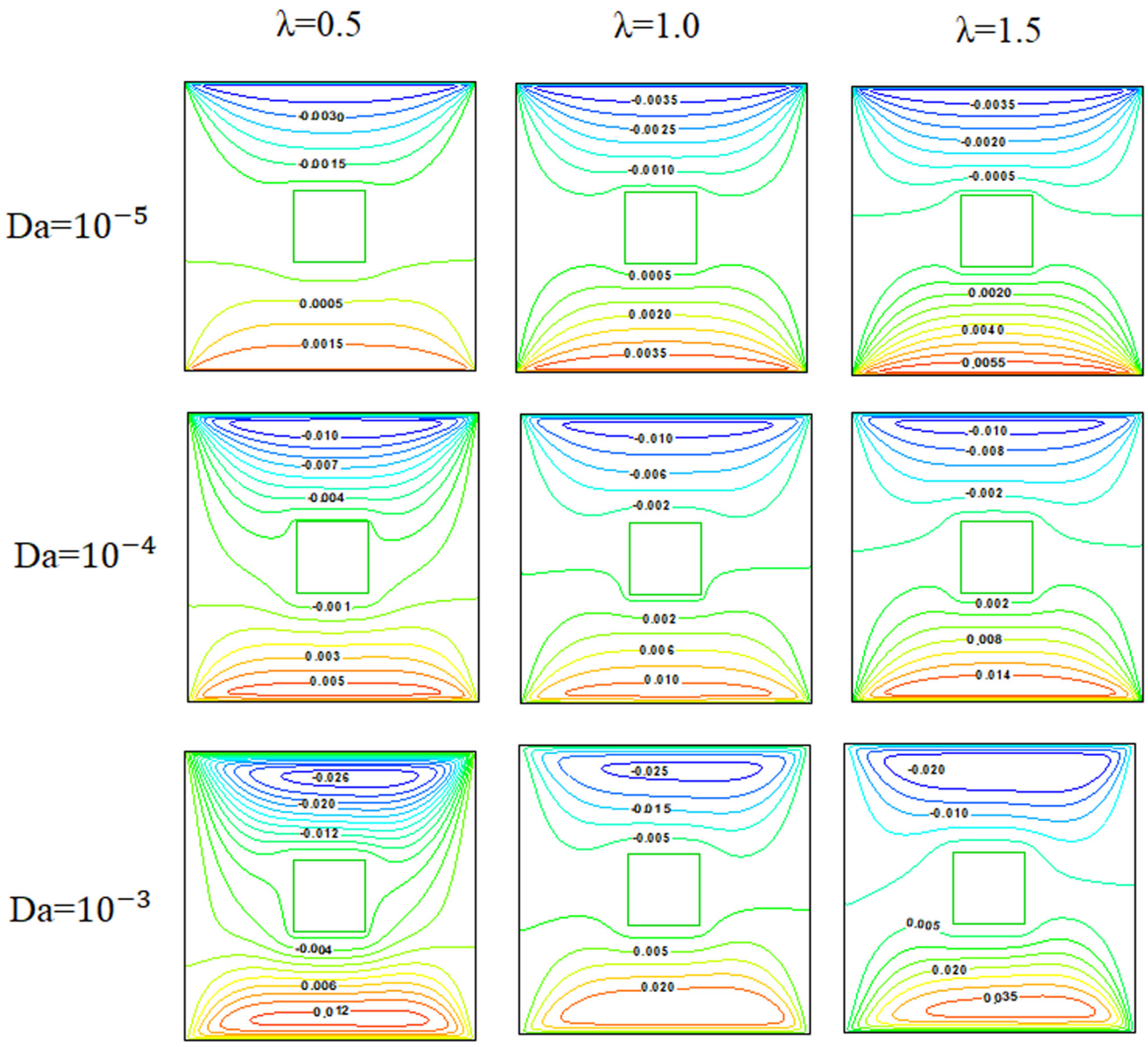


**Figure 7:** Demonstration of steady state streamlines subject to velocity wall ratio and Darcy number when $\phi$ = 0.025 and Ri = 1.0.

rate of clockwise cells. The heat transfer process is also influenced by the Darcy number, with higher values indicating stronger convection due to increased buoyancy force. This effect is observed across all wall speed ratios. Additionally, as the wall velocity ratio rises, the isotherms near the bottom position distort and shift towards the top wall.

Isotherms contours and streamlines for the escalating estimations of velocity wall ratio ($\lambda < 0$) is displayed in Figure 9, when $\phi = 0.025$, Da = $10^{-3}$, and Ri = 0.01. A velocity wall ratio ($\lambda < 0$) indicates that the top and bottom walls are moving in opposite directions. In this case, the top wall moves steadily to the right with constant velocity ($U_0 = 1$), while the bottom wall moves erratically to the left with a variable velocity ($U_0 = -\lambda$). In this scenario, a negative $\lambda$ value indicates that shear and buoyancy forces are working together. When $\lambda = 0.5$, the entire cavity is filled with a single clockwise cell containing multiple structures, resulting in eddies forming near the top and bottom walls. The figure shows that the eddies near the top wall are more concentrated and powerful compared to those near the bottom wall, with the dominant velocity at the top wall being ($U_t = 1$) and at the bottom wall being $U_b = -0.5$. As the bottom wall velocity increases towards the left, the eddies near the bottom wall gradually reinforce in both flow rate and size.

For a low wall velocity ratio, the distribution of isotherms in the cavity can be observed. Isotherms near the hot wall move right, while those near the cold wall move left due to the opposite motion of the horizontal walls.

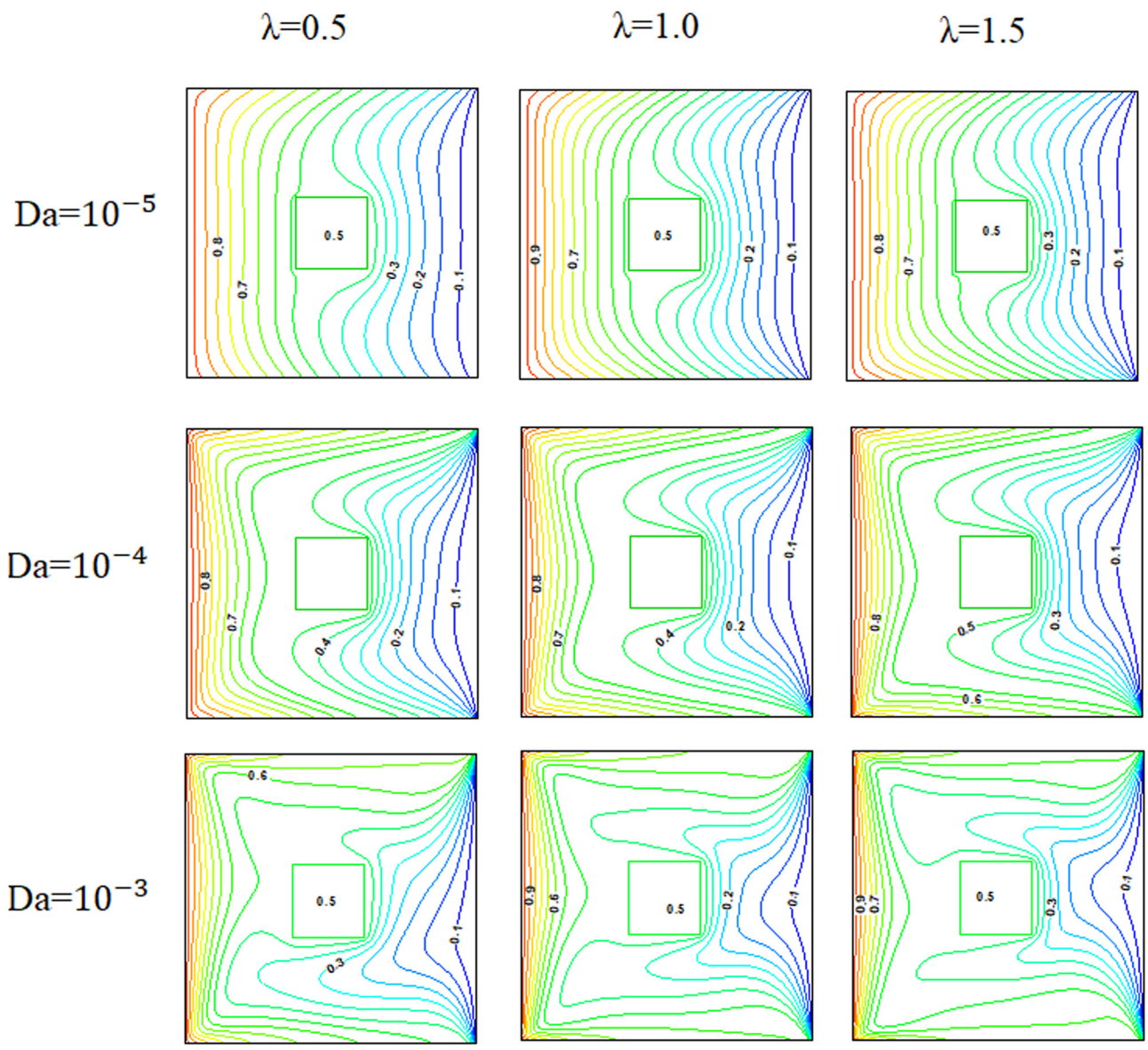


**Figure 8:** Demonstration of isotherms subject to velocity wall ratio and Darcy number when $\phi$ = 0.025 and Ri = 1.

These isotherms generally follow the path of the bottom wall, and they are more spread out near the bottom wall compared to the top wall. This difference is due to the stronger shear force experienced at the top wall. As the wall velocity ratio increases, leading to higher shear force along the bottom wall, the distribution of isotherms near the bottom wall becomes distorted, as anticipated.

Figure 10 is sketched for both vertical as well as horizontal velocity distributions for the rising estimations of Ri when $\lambda$ = 1, Da = $10^{-3}$, and $\phi$ = 0.025. The velocities of forced and mixed convection regions (Ri = 0.01, 1.0), are almost same at the mid-section of the cavity. Nevertheless, the natural convection with a dominant Richardson number of 100 results in the highest velocity at the center plane when compared to Richardson numbers of 0.01 and 1.0. Figure 11 highlights the interpretation of mid-height velocity components for both horizontal and vertical direction for rising values of Darcy number. As the Da values increase, the speed observed also increases, as depicted in Figure 11. The velocity remains relatively constant for Da = $10^{-5}$ & $10^{-4}$ in the mid-plane of the cavity. Furthermore, the velocities remain constant at the core for all Da, which is attributed to the solid block's presence (Tables 2 and 3).

Figure 12 illustrates the fields of mid-height velocity components for various wall velocity ratios in both horizontal and vertical directions. The horizontal velocities display an upsurge with higher wall speed ratios. Meanwhile,

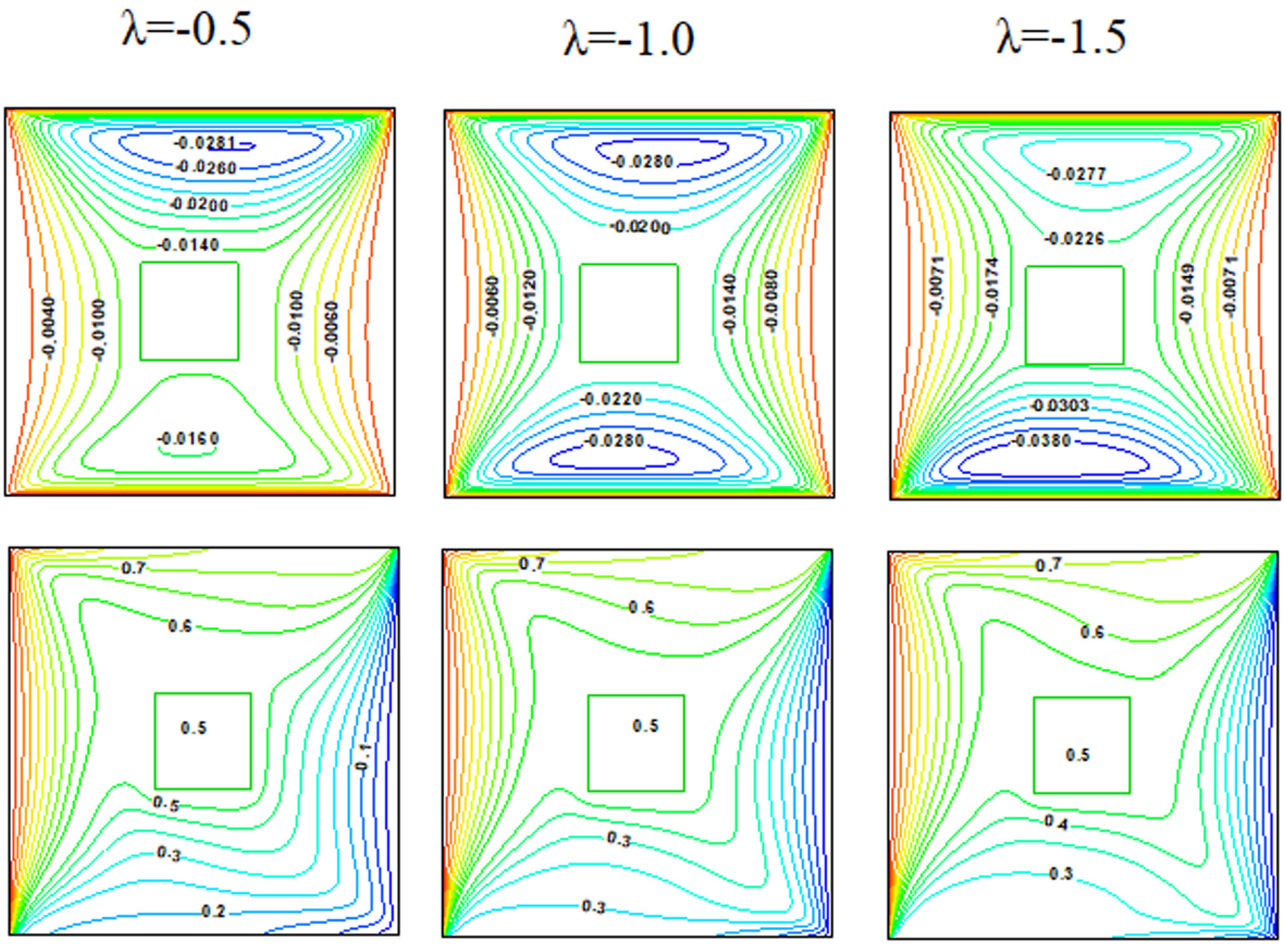


**Figure 9:** Physical interpretation of steady state streamlines and isotherms subject to wall velocity ratio when $\phi$ = 0.025, Ri = 0.01, and Da = $10^{-3}$.

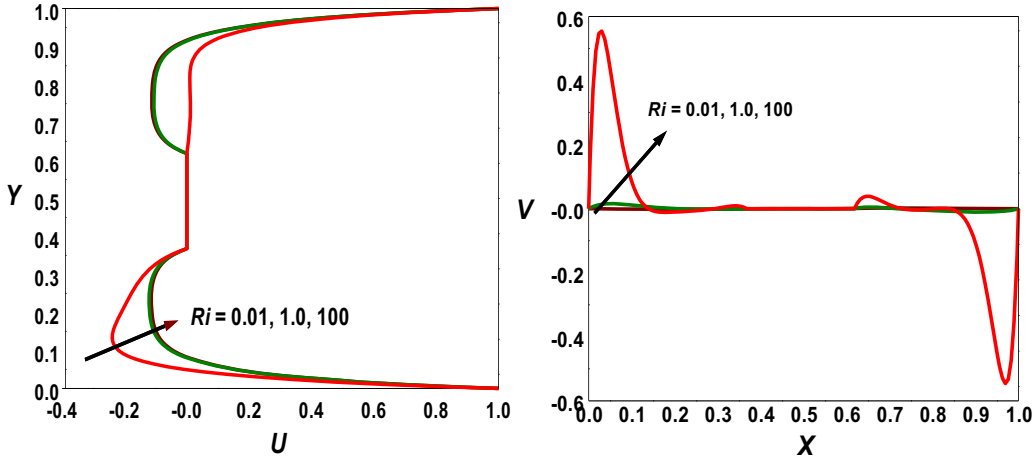


**Figure 10:** Vertical velocity and mid-height vertical and horizontal velocity profiles subject to Ri when Da = $10^{-3}$, $\phi$ = 0.025, and $\lambda$ = 1.

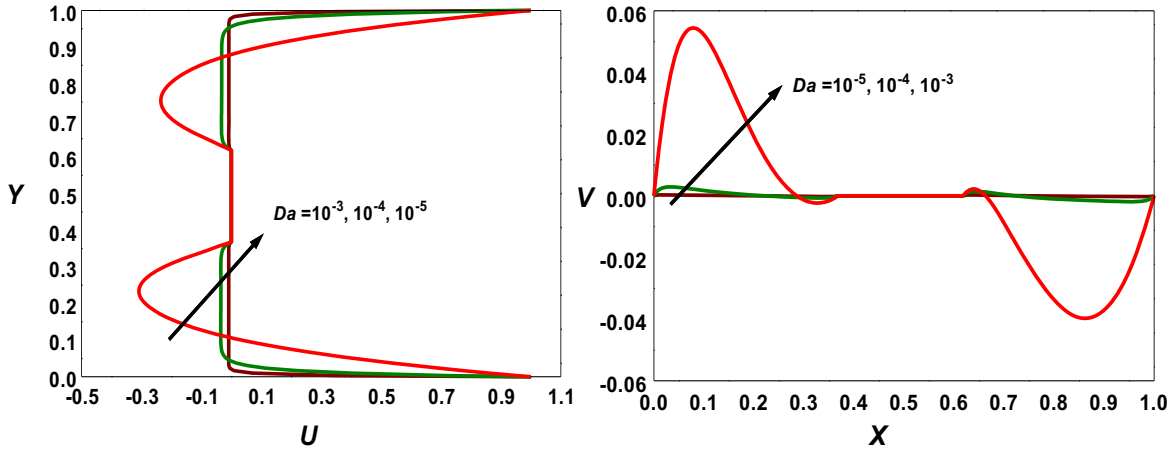


**Figure 11:** Vertical velocity and mid-height horizontal velocity against Darcy number when $\phi$ = 0.025, Ri = 1.0, and $\lambda$ = 1.

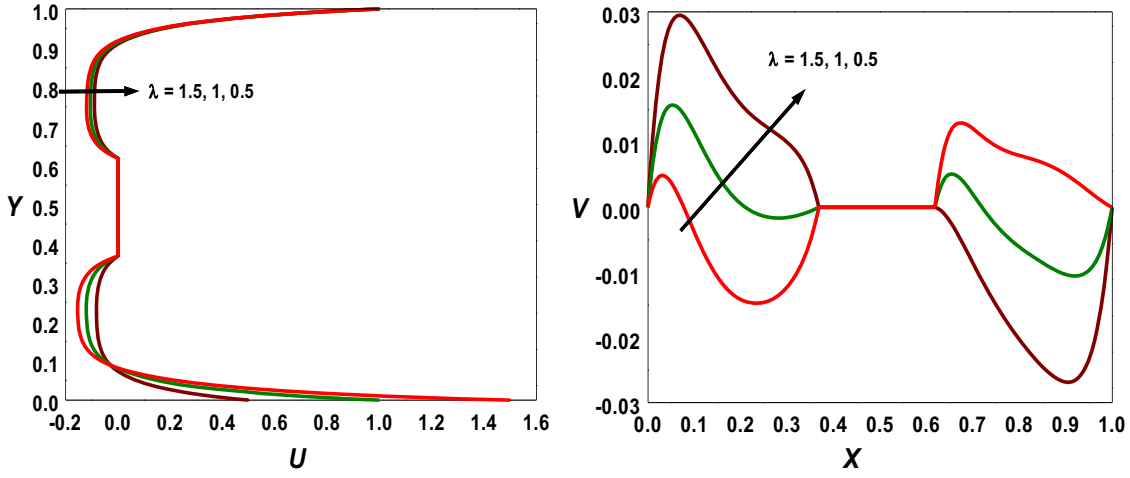


**Figure 12:** Vertical velocity and mid-height horizontal velocity against wall velocity ratio when $\phi$ = 0.025, Ri = 1.0, and Da = $10^{-3}$.

the V-velocity fields show two separate patterns at the mid-plane of the cavity. On the left side, a low wall speed ratio outcomes in higher V-velocity magnitude, while on the right side, a high wall speed ratio leads to maximum velocity due to augmented shear forces in that direction. In Figure 13(a) and (b), the time history of the average Nusselt number for various Richardson (Ri) and Darcy (Da) numbers is presented. Initially, the average Nusselt number is high and gradually declines over time until reaching a steady state. It is observed that the region dominated by forced convection (Ri = 0.01) and the region dominated by conduction Da = $10^{-5}$ take the longest time to reach steady state solutions.

Tables 5 and 6 display the dissimilarity average Nusselt number for increasing estimations of Ri, $\lambda$, and $\phi$ when Da = $10^{-3}$. From the definition of Richardson number (Ri = $\frac{\text{Gr}}{\text{Re}^2}$), we can say that the increase in Ri leads to an augmentation of Gr since Re is fixed and thus enhances the natural convection. For this reason, the heat transport rate upsurges with the increase in the Richardson number. The observation confirmed the augmented rate of heat transport due to the enrichment of the base liquid with Cu nanoparticles. In addition, for all the values of Ri, increasing wall speed ratio either in same direction or opposite direction the heat transport rate is augmented. At high Ri and solid volume fraction (Ri = 100, $\phi$ = 0.05), the significance of heat transport rate is augmented by 6% only with the upsurge of $-\lambda$ from 0.5 to 1.5; however, there was a 29% increase in the rate of heat transfer when the Richardson number was low (Ri = 0.01). Similarly, the heat transport rate amplified by only 5% with the upsurge of $\lambda$ from 0.5 to 1.5 at high Ri, $\phi$ whereas the rate of heat transfer increases by 28% when the Richardson number

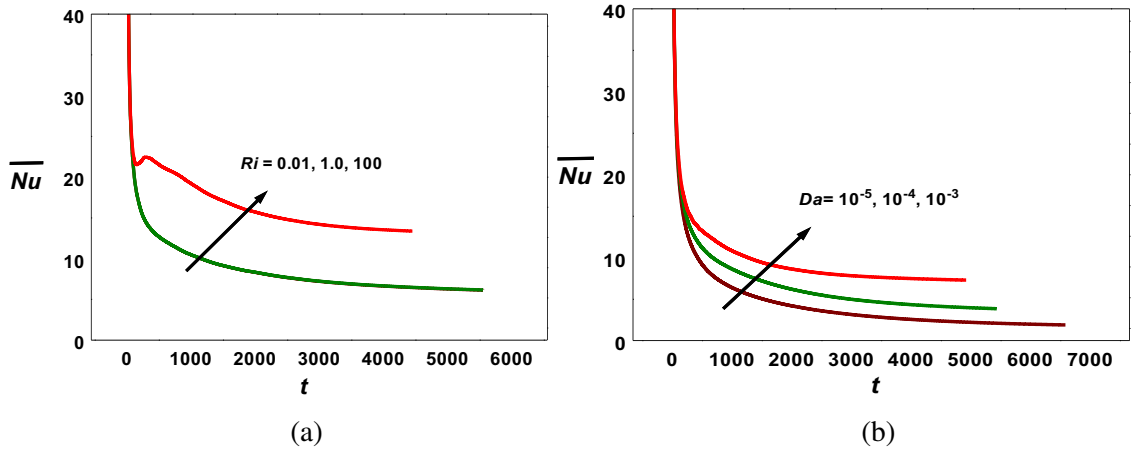


**Figure 13:** The time history of average Nusselt number for (a) different Ri with fixed Da = $10^{-3}$, $\phi$ = 0.025 (b) different Da with fixed Ri = 1.0, $\phi$ = 0.025.

**Table 5:** Examination of $\overline{\mathrm{Nu}}$ subject to Richardson number, wall speed ratio ($\lambda < 0$), and $\phi$ at Da = $10^{-3}$

| Richardson number | Nanoparticles volume fraction | $\overline{\mathrm{Nu}}$ | | |
|---|---|---|---|---|
| | | $\lambda$ | | |
| | | −0.5 | −1 | −1.5 |
| 0.01 | 0 | 5.919057 | 6.947259 | 7.654598 |
| | 0.025 | 6.065295 | 7.180177 | 7.947156 |
| | 0.05 | 6.206901 | 7.407756 | 8.234361 |
| 1.0 | 0 | 6.214299 | 7.148318 | 7.812973 |
| | 0.025 | 6.357829 | 7.381020 | 8.104932 |
| | 0.05 | 6.494800 | 7.608253 | 8.392443 |
| 100 | 0 | 13.38110 | 13.77049 | 14.09873 |
| | 0.025 | 13.68186 | 14.10407 | 14.45983 |
| | 0.05 | 13.96672 | 14.42297 | 14.80826 |

**Table 6:** Examination of $\overline{\mathrm{Nu}}$ *vs* Richardson number, wall speed ratio ($\lambda < 0$) and $\phi$ at Da = $10^{-3}$

| Richardson number | Nanoparticles volume fraction | $\overline{\mathrm{Nu}}$ | | |
|---|---|---|---|---|
| | | $\lambda$ | | |
| | | 0.5 | 1 | 1.5 |
| 0.01 | 0 | 5.196048 | 5.978574 | 6.636054 |
| | 0.025 | 5.284909 | 6.129442 | 6.797601 |
| | 0.05 | 5.371582 | 6.227012 | 6.960791 |
| 1.0 | 0 | 5.376878 | 6.011653 | 6.544033 |
| | 0.025 | 5.446927 | 6.157492 | 6.714101 |
| | 0.05 | 5.515021 | 6.300520 | 6.884848 |
| 100 | 0 | 12.71778 | 13.12886 | 13.40783 |
| | 0.025 | 12.95839 | 13.37671 | 13.69086 |
| | 0.05 | 13.18089 | 13.60192 | 13.95060 |

is low (Ri = 0.01). This clearly shows that as the value of $\lambda$ increases, the forced convection region produces the highest heat transfer rate.

Tables 7 and 8 are sketched to determine how some variables, *i.e.*, Da, $\lambda$, and $\phi$ influence the Nusselt number when Ri is constant. Looking at the figures, a better heat flow (Nusselt number or heat transfer coefficient) can be seen if Da, $\phi$, and $|\lambda|$ are assigned larger values. Examination of the tables shows a better heat transfer rates for negative $\lambda$ values compared to positive $\lambda$ values. This result shows that the opposite moving walls generate the effective cooling system than the same direction of moving walls. In addition to that the increasing percentage of heat transport rate is sufficiently large by upsurge of wall speed ratio than the rising of solid volume fraction. At the moderate value of Da ($10^{-4}$), the heat transport rate is improved by 46% with the enhancement of $|\lambda|$ from 0.5 to

**Table 7:** Examination of $\overline{\mathrm{Nu}}$ *vs* Darcy number, wall speed ratio ($\lambda < 0$) and $\phi$ at Ri = 1.0

| Darcy number | Nanoparticles volume fraction | $\overline{\mathrm{Nu}}$ | | |
|---|---|---|---|---|
| | | $\lambda$ | | |
| | | −0.5 | −1 | −1.5 |
| $10^{-5}$ | 0 | 1.880017 | 2.101634 | 2.363503 |
| | 0.025 | 1.947787 | 2.161028 | 2.415158 |
| | 0.05 | 2.021530 | 2.226617 | 2.473001 |
| $10^{-4}$ | 0 | 3.612986 | 4.512475 | 5.260185 |
| | 0.025 | 3.649016 | 4.561086 | 5.338616 |
| | 0.05 | 3.687500 | 4.608705 | 5.412831 |
| $10^{-3}$ | 0 | 6.214299 | 7.148318 | 7.812973 |
| | 0.025 | 6.357829 | 7.381020 | 8.104932 |
| | 0.05 | 6.494800 | 7.608253 | 8.392443 |

**Table 8:** Examination of $\overline{\mathrm{Nu}}$ *vs* Da, wall speed ratio ($\lambda < 0$) and $\phi$ at Ri = 1.0

| Darcy number | $\phi$ | $\overline{\mathrm{Nu}}$ | | |
|---|---|---|---|---|
| | | $\lambda$ | | |
| | | **0.5** | **1** | **1.5** |
| $10^{-5}$ | 0 | 1.732055 | 1.841868 | 2.007792 |
| | 0.025 | 1.802991 | 1.903395 | 2.059767 |
| | 0.05 | 1.880220 | 1.971709 | 2.119037 |
| $10^{-4}$ | 0 | 3.133966 | 3.852411 | 4.444283 |
| | 0.025 | 3.154937 | 3.862300 | 4.464971 |
| | 0.05 | 3.181067 | 3.874341 | 4.484497 |
| $10^{-3}$ | 0 | 5.376878 | 6.011653 | 6.544033 |
| | 0.025 | 5.446927 | 6.157492 | 6.714101 |
| | 0.05 | 5.515021 | 6.300520 | 6.884848 |

1.5 than the remaining values of Da($10^{-5}, 10^{-3}$). At higher Darcy number (Da = $10^{-3}$) and low wall velocity ratio $\lambda$ = 0.5(−0.5), the heat transport rate is enhanced by only 3% (4%) with the enhancement of nanoparticles concentration from 0 to 0.05 whereas it is increased to about 9% (8%) at low (Da = $10^{-5}$). However, the opposite behavior was found at high wall velocity ratio $\lambda$ = 1.5(−1.5). This indicates that the influence of nanoparticle concentration is more efficient in the conduction conquered region (Da = $10^{-5}$) when low value of wall velocity is very low, whereas the convection conquered region (Da = $10^{-3}$) is more efficient for high value of wall velocity ratio.

# 5 Final remarks

In this research attempt, we have investigated the issue of mixed convective heat transport of nanofluids in a permeable cavity with an isothermal solid block, using numerical analysis. We have varied the wall speed ratio and concluded the following findings from our research:

- The non-dimensional parameters, *i.e.*, Ri, Da, and $\lambda$ have a significant impact on both the flow and thermal fields.
- The heat transport rate is enhanced for the higher values of Ri, Da, $\varphi$, and $|\lambda|$.
- A faster rate of heat transport is noticed when the wall velocity ratio $\lambda < 0$ compared to $\lambda > 0$. This indicates that supremum heat transport occurs when the lids move in opposite directions rather than in the same direction.
- At high Ri = 100 and $\phi$ = 0.05, the heat transport rate enhanced by only 6% (5%) when the parameter $-\lambda$ ($\lambda$) was increased from 0.5 to 1.5. In contrast, at Ri = 0.01, the heat transport rate enhanced by 29% (28%).
- At higher (Da = $10^{-3}$) and low wall velocity ratio $\lambda$ = 0.5(−0.5), the heat transfer rate increased by only 3% (4%) when the nanoparticle concentration was increased from 0 to 0.05. However, at lower (Da = $10^{-5}$), the heat transport rate enhanced by approximately 9% (8%).
- After taking into account all the elements that improve the transfer of heat, it was determined that the best rate of heat transfer in the existing system is attained with the specific combination of parameters (Ri, Da, $\varphi$, and $|\lambda|$) = (100, $10^{-3}$, 0.05, and 1.5).
- For future research, it is recommended to inspect the consequence of a magnetic field on heat transport, as well as study the inspiration of the location and size of the isothermal solid block.

**Acknowledgments:** Researchers Supporting Project number (RSPD2024R576), King Saud University, Riyadh, Saudi Arabia.

**Funding information:** Researchers Supporting Project number (RSPD2024R576), King Saud University, Riyadh, Saudi Arabia.

**Author contributions:** All authors have accepted responsibility for the entire content of this manuscript and approved its submission.

**Conflict of interest:** The authors state no conflict of interest.

# References

[1] Javed T, Siddiqui MA. Effect of MHD on heat transfer through ferrofluid inside a square cavity containing obstacle/heat source. Int J Therm Sci. 2018;125:419–27.

[2] Sun H, Chnier E, Lauriat G. Effect of surface radiation on the breakdown of steady natural convectionflows in a square, air-filled cavity containing a centered inner body. Appl Therm Eng. 2011;31:1252–62.

[3] Kalidasan K, Velkennedy R, RajeshKanna P. Laminar natural convection of Copper - Titania/Water hybrid nanofluid in an open ended C-shaped enclosure with an isothermal block. J Mol Liq. 2017;246:251–8.

[4] Mehmood K, Hussain S, Sagheer M. Mixed convection in alumina-water nanofluid filled lid-driven square cavity with an isothermally heated square blockage inside with magnetic field effect: Introduction. Int J Heat Mass Transf. 2017;109:397–409.

[5] Haq RU, Soomro FA, Hammouch Z. Heat transfer analysis of CuO-water enclosed in a partially heated rhombus with heated square obstacle. Int J Heat Mass Transf. 2018;118:773–84.

[6] Kumar DS, Dass AK, Dewan A. Analysis of non-Darcy models for mixed convection in a porous cavity using multigrid approach. Numer Heat Transf Part A. 2009;56:685–708.

[7] Sivasankaran S, Pan KL. Numerical simulation on mixed convection in a porous lid-driven cavity with nonuniform heating on both side walls. Numer Heat Transf Part A. 2012;61:101–21.
[8] Moria H. Natural convection in an L-shape cavity equipped with heating blocks and porous layers. Int Commun Heat Mass Transf. 2021;126:105375.
[9] Colak E, Ekici O, Oztop HF. Mixed convection in a lid-driven cavity with partially heated porous block. Int Commun Heat Mass Transf. 2021;126:105450.
[10] Fu Y, Bian B, Liu Y, Zhang L, Li M, Wen J, et al. Airside heat transfer analysis using Wilson plot method of three analogous serpentine tube heat exchangers for aero-engine cooling. Appl Therm Eng. 2024;248:123238.
[11] Xiao D, Xiao H, Song W, Li G, Zhang J, Deng H, et al. Utilization method of low-grade thermal energy during drilling based on insulated drill pipe. Renew Energy. 2024;225:120363.
[12] Hou Y, Cheng M, Sheng Z, Wang J. Unsteady conjugate heat transfer simulation of wall heat loads for rotating detonation combustor. Int J Heat Mass Transf. 2024;221:125081.
[13] Begum AS, Nithyadevi N, Oztop HF, Al-Salem K. Numerical simulation of MHD mixed convection in a nanofluid filled non-Darcy porous enclosure. Int J Mech Sci. 2017;130:154–66.
[14] Hussain S, Mehmooda K, Sagheera M, Farooqa A. Entropy generation analysis of mixed convective flow in an inclined channel with cavity with $Al_2O_3$-water nanofluid in porous medium. Int Commun Heat Mass Transf. 2017;89:1054–66.
[15] Nithyadevi N, Begum AS, Oztop HF, Abu-Hamdeh N. Mixed convection analysis in heat transfer enhancement of a nanofluid filled porous enclosure with various wall speed ratios. Int J Heat Mass Transf. 2017;113:716–29.
[16] Alomari MA, Al-Farhany K, Al-Salami QH, Al-Jaburi K, Alyousuf FQA, Ali IR, et al. Magnetohydrodynamic mixed convection in lid-driven curvilinear enclosure with nanofluid and partial porous layer. J Magn Magn Mater. 2023;582:170952.
[17] Long X, Chong K, Su Y, Du L, Zhang G. Connecting the macroscopic and mesoscopic properties of sintered silver nanoparticles by crystal plasticity finite element method. Eng Fract Mech. 2023;281:109137.
[18] Nguyen MT, Aly AM, Lee SW. Natural convection in a non-Darcy porous cavity filled with Cu-water nanofluid using the characteristic-based split procedure in finite element method. Numer Heat Transf Part A. 2015;67:224–47.
[19] Jmai R, Ben-Beya B, Lili T. Numerical analysis of mixed convection at various wall speed ratios in two sided lid-driven cavity partially heated and filled with nanofluid. J Mol Liq. 2016;221:691–713.
[20] Patankar SV. Numerical heat transfer and fluid flow. Washington: Hemisphere Publishing Corporation; 1980.